Transferrin receptor serves a role in promoting PANoptosis in thyroid cancer

SHUNGAO MA[1], ZHIQIANG MA[1], JINGWEI SHEN[1], HONG LIU[1], HUA YANG[1], YUQIN HU[2] and SIMENG YING[2]

[1]Department of Clinical Laboratory, Dali Bai Autonomous Prefecture People's Hospital, Dali, Yunnan 671000, P.R. China; [2]Health Science Center, Dali University, Dali, Yunnan 671000, P.R. China

Received March 27, 2025; Accepted October 22, 2025

DOI: 10.3892/ol.2025.15394

Abstract. PANoptosis is an emerging form of regulated cell death (RCD) that results from the interaction between necrosis, apoptosis and pyroptosis. The transferrin receptor (TFRC) is a suppressor in thyroid cancer (TC) and is involved in several RCD pathways, including ferroptosis, apoptosis, cuproptosis and necrosis. The present study aimed to assess how TFRC influences PANoptosis in TC and evaluate its underlying molecular mechanisms. Bioinformatics analyses were performed to identify coding genes associated with the expression of PANoptosis markers (Z-DNA-binding protein 1 and absent in melanoma 2) in The Cancer Genome Atlas-Thyroid Cancer (TCGA-THCA) dataset. Techniques such as PI/Calcein-AM and YO-PRO-1/PI staining, and western blotting were used to assess how TFRC influences PANoptosis in TC cells. Additionally, mRNA sequencing (mRNA-seq) was employed to identify differentially expressed (DE)-mRNA associated with TFRC. A total of 729 and 1,568 coding genes in the TCGA-THCA dataset demonstrated a significant association with ZBP-1 and AIM2 expression, respectively, involving regulation of immunity, apoptosis and necroptosis. Among these, TFRC was identified as a prognostic biomarker for TC and was downregulated in TC tissues and cells. Overexpression of TFRC increased TC cells undergoing pyroptosis, apoptosis and necroptosis, whilst it decreased the number of viable cells. Additionally, TFRC overexpression was associated with an elevation in the expression of cleaved-caspase (CASP)1, CASP1, cleaved-CASP3, CASP3, phospho-mixed lineage kinase domain-like and total-receptor-interacting serine/threonine-protein kinase 3, whereas TFRC knockdown was associated with the opposite effects. mRNA-seq identified 828 DE-mRNAs associated with TFRC. Enrichment analysis revealed that these DE-miRNAs regulate cell cycle, apoptosis, necrotic apoptosis, pyroptosis, oxidative stress and immunity. Furthermore, in the protein-protein interaction network constructed from DE-mRNAs, genes such as *CD34*, lactate dehydrogenase A (*LDHA*) and low-density lipoprotein receptor (*LDLR*) were identified as TFRC-interacting partners, and their expression demonstrated a positive association with TFRC. Furthermore, TFRC knockdown effectively reduced the levels of these genes. In conclusion, TFRC facilitates PANoptosis in TC, potentially through interactions with genes such as *CD34*, *LDHA* and *LDLR*.

Correspondence to: Professor Zhiqiang Ma, Department of Clinical Laboratory, Dali Bai Autonomous Prefecture People's Hospital, 35 Renmin South Road, Dali, Yunnan 671000, P.R. China
E-mail: 13708661212@163.com

Key words: thyroid cancer, PANoptosis, bioinformatics, RNA sequence, transferrin receptor

Introduction

Thyroid cancer (TC) is a common endocrine malignancy comprising anaplastic thyroid carcinomas (ATC), medullary thyroid carcinoma and differentiated thyroid carcinoma (DTC) (1). Globally, there are ~586,202 new cases of TC and 43,646 deaths associated with it, ranking ninth in incidence among all cancers. Furthermore, it is expected to overtake colorectal cancer as the fourth most prevalent cancer in the USA by 2030 (2,3). Among the subtypes of TC, DTC accounts for ~95% of cases and generally has a favorable prognosis, whereas ATC is rare but aggressive, with a median survival of <6 months (4).

Radioactive iodine ablation continues to be the primary treatment for TC (5); however, it is ineffective in all ATC cases and in ~10% of DTC cases (5). This is due to resistance caused by changes in the MAPK and PI3K pathways, as well as mutations or rearrangements in B-Raf proto-oncogene, serine/threonine kinase, neurotrophic receptor tyrosine kinase, telomerase reverse transcriptase, RAS proto-oncogene, GTPase, anaplastic lymphoma kinase and ret proto-oncogene in ATC and DTC, which serve as important diagnostic and prognostic markers for TC (4,6). Targeted inhibitors against these biomarkers, such as sorafenib, lenvatinib and vemurafenib, have thus become promising strategies for treating ATC and DTC; however, targeted therapies face challenges, including limited effectiveness, drug resistance and serious side effects (4,6). Therefore, further research into TC molecular mechanisms is necessary to develop more effective targeted treatment strategies.

Inducing tumor cell death is a fundamental aspect of developing cancer treatments. For decades, apoptosis, pyroptosis and necroptosis were regarded as separate cell death pathways. More recently, PANoptosis has been described as an integrated inflammatory cell death process involving crosstalk among pyroptosis, apoptosis and necroptosis, coordinated by multiprotein complexes called PANoptosomes (7-11). PANoptosis begins when pathogen- and damage-associated molecular patterns activate the pattern recognition receptors Z-DNA-binding protein 1 (ZBP1) and absent in melanoma 2 (AIM2). Once activated, ZBP1 and AIM2 recruit adaptor proteins with protein-interaction domains to form PANoptosomes, which contain key effectors of apoptosis, pyroptosis and necroptosis, including caspase (CASP)1/3/8/9, dasdermin D, receptor interacting serine/threonine kinase 3 (RIPK3) and mixed lineage kinase domain like pseudokinase (MLKL). Within these structures, the coordinated action of these effectors causes rupture of the plasma membrane and organelle membranes, initiating cascades of inflammatory and immune responses. Notably, PANoptosis has been associated with several malignancies, including esophageal cancer (12), melanoma (13), adrenocortical carcinoma (14) and diffuse large B-cell lymphoma (15). Specifically, sulconazole has been reported to increase the radiosensitivity of esophageal cancer by inducing PANoptosis (12). Adenosine deaminase RNA specific 1 and CDK1 also facilitate tumor burden in colorectal cancer, melanoma and adrenocortical carcinoma by suppressing ZBP1-mediated PANoptosis (13,14). Furthermore, suppression of SAM and HD domain containing deoxynucleoside triphosphate triphosphohydrolase 1 has been reported to stimulate PANoptosis by activating stimulator of interferon response CGAMP interactor, which effectively alleviates diffuse large B-cell lymphoma (15). Its role in influencing the tumor immune microenvironment emphasizes its potential for therapy. Nonetheless, the regulatory mechanisms and critical molecular factors governing PANoptosis in TC are still unknown, marking a substantial gap in current knowledge.

The transferrin receptor (TFRC) is a transmembrane glycoprotein dimer widely expressed on the cell membrane and mainly involved in cellular iron uptake (16). Due to its role in iron homeostasis, TFRC has been reported to promote ferroptosis in several cancers, including TC (17-19), endometrial carcinoma (20), colorectal carcinoma (21), hepatocellular carcinoma (22) and gastric carcinoma (23). For example, high TFRC expression has been reported to predict a worse prognosis in patients with TC, compared with low TFRC expression (17,18), and it interacts with longevity assurance homolog 2 to promote ferroptosis in TC (19). In addition to ferroptosis, TFRC has been associated with numerous cell death types such as apoptosis, pyroptosis, cuproptosis, autophagy and necrosis (24-26). Specifically, TFRC promotes PTEN induced kinase 1 (PINK1)-parkin RBR E3 ubiquitin protein ligase-dependent mitochondrial autophagy and apoptosis in anaplastic large cell lymphoma (24). Notably, TFRC-mediated cell death displays features similar to PANoptosis. Overall, the aforementioned studies imply that TFRC could serve as a molecular regulator of PANoptosis.

The present study aimed to identify biomarkers associated with ZBP1 and AIM2 expression in the TCGA-THCA cohort and determine their prognostic value in TC. Furthermore, the present study intended to investigate the utility of the prognostic biomarker as a target in TC and of the expression of ZBP1 and AIM2 on PANoptosis using *in vitro* experiments and to characterize the molecular mechanisms that may be involved with this target using mRNA-seq. It aims to provide a new perspective and a solid experimental basis for the development of therapeutic strategies related to PANoptosis in TC.

Materials and methods

PANoptosis-related bioinformatics analysis. The TCGA-THCA dataset was obtained from TCGA (https://portal.gdc.cancer.gov), which includes 571 samples with clinical data from the study by Liu *et al* (27). The dataset features RNA-sequencing (RNA-seq) expression profiles (transcripts per million format) of 59 paracancerous samples and 507 tumor samples. Pearson correlation analysis identified coding genes associated with ZBP1 and AIM2 expression across 571 RNA-seq datasets. Coding genes with an adjusted P-value (P.adj) <0.05 were determined to be significantly associated with ZBP1 and AIM2 expression. The clusterProfiler package (v4.4.4) (28) in R was used to perform Gene Ontology (GO) and Kyoto Encyclopedia of Genes and Genomes (KEGG) enrichment analysis of these co-associated coding genes to assess their roles in molecular composition, biological processes, molecular functions and signaling pathways. The STRING database (29) and Cytoscape software (v3.7.2) (30) were used to construct and visualize the protein-protein interaction (PPI) networks of ZBP1- and AIM2-associated coding genes, and the resulting PPIs were analyzed using the Network Analysis and MCODE (31) apps within Cytoscape software. Finally, the survival package (v3.3.1) (32) in R software was used to performed log-rank tests and univariate and multivariate Cox regression analyses to assess the associations between ZBP1- and AIM2-associated coding genes and patient prognosis in TC.

Culture and transfection of TC cells. Normal human thyroid cells (Nthy) and TC cell lines (K1, TPC-1 and BCPAP) were purchased from Procell Life Science & Technology Co., Ltd. and Wuhan SAIOS Biotechnology Co., Ltd. All cell lines underwent DNA amplification using the 21-short tandem repeat (STR) profiling protocol, followed by detection of STR loci and the sex-determining gene *Amelogenin* on a SeqStudio™ Genetic Analyzer (Thermo Fisher Scientific, Inc.). DNA profiles of Nthy, K1, TPC-1 and BCPAP cells matched reference profiles of cell lines in the ExPASy database (https://www.expasy.org/), with accession numbers CVCL-2659, CVCL-2537, CVCL-6298 and CVCL-0153, respectively.

Nthy, TPC-1 and BCPAP cells were cultured in RPMI 1640 medium (cat. no. 61870-127; Gibco; Thermo Fisher Scientific, Inc.) supplemented with 1% double antibodies (cat. no. PB180120; Procell Life Science & Technology Co., Ltd.) and 10% FBS (cat. no. 12003C; Merck KGaA) at 5% CO_2 and 37˚C, whereas K1 cells were maintained in Ham's F-12K medium (cat. no. 21127-022; Gibco; Thermo Fisher Scientific, Inc.) at 5% CO_2 and 37˚C.

For genetic manipulation, Genomeditech (Shanghai) Co., Ltd. synthesized short hairpin (sh)RNA constructs targeting *TFRC* for knockdown and provided the PGMLV-CMV-MCS-EF1-ZsGreen1-T2A-Puro plasmid for overexpression of *TFRC*. The shRNA sequences targeting TFRC used were as follows: 5'-CGTGAATTTAAACTC AGCAAA-3' (shRNA sense #1); 5'-TTTGCTGAGTTTAAA TTCACG-3' (shRNA antisense #1); 5'-GCCAGCTTTACT GGAGAACTT-3' (shRNA sense #2); 5'-AAGTTCTCCAGT AAAGCTGGC-3' (shRNA antisense #2); 5'-GCTGGTCAG TTCGTGATTAAA-3' (shRNA sense #3); 5'-TTTAATCAC GAACTGACCAGC-3' (shRNA antisense #3); 5'-TTCTCC GAACGTGTCACGT-3' [negative control (NC) sense]; and 5'-ACGTGACACGTTCGGAGAA-3' (NC antisense). BCPAP cells were randomized into overexpression control (OV-NC) and overexpression of TFRC (OV-TFRC) groups, whilst K1 cells were randomized into knockdown control (KD-NC) and knockdown of TFRC (KD-TFRC) groups. Transfections were performed using Lipo8000™ transfection reagent (cat. no. C0533-7.5 ml; Beyotime Institute of Biotechnology), with BCPAP cells transfected with *TFRC* overexpression plasmid or its NC (blank PGMLV-CMV-MCS-EF1-ZsGreen1-T2A-Puro plasmid) and K1 cells transfected with *TFRC* shRNA or its NC (oligo control).

Cellular PANoptosis-related staining assays. The PI/Calcein-AM Double Staining Kit (cat. no. CA1630; Beijing Solarbio Science & Technology Co., Ltd.) and Apoptosis and Necrosis Detection Kit with YO-PRO-1 and PI Kit (cat. no. C1075S; Beyotime Institute of Biotechnology) were used to assess PANoptosis in BCPAP and K1 cells. For PI/Calcein-AM staining, BCPAP and K1 cells were adjusted to a concentration of $1x10^5$ cells/ml using 1X assay buffer and incubated with Calcein-AM for 25 min at 37˚C, followed by PI for 5 min at 37˚C. For YO-PRO-1/PI staining, PBS-washed BCPAP and K1 cells ($5x10^4$ cells/ml) were inoculated in 24-well plates, and 100 μl YO-PRO-1 and PI staining was added to each well for 20 min at 37˚C. Representative images of PI/Calcein-AM and YO-PRO-1/PI staining were captured using a BX53 fluorescence microscope (Olympus Corp.). Excitation filters were set at 535 nm for PI (red), 495 nm for Calcein-AM (green) and 491 nm for YO-PRO-1 (green), enabling the detection of apoptosis/necroptosis, viable cells and necroptosis/pyroptosis, respectively.

Western blot assay for PANoptosis markers. Total proteins were extracted from BCPAP and K1 cells using RIPA lysis buffer (cat. no. C500005; Sangon Biotech Co., Ltd.). Protein concentrations were determined using a BCA Protein Colorimetric Assay Kit (cat. no. E-BC-K318-M; Elabscience®; Elabscience Bionovation Inc.), separated using a 5 and 10% SDS-PAGE gel kit (cat. no. P1200; Beijing Solarbio Science & Technology Co., Ltd.) and transferred onto PVDF membranes (cat. no. 88520; Thermo Fisher Scientific, Inc.). The mass of protein loaded per lane was 20 μg. Membranes were blocked with 5% skimmed milk at room temperature for 1 h and incubated with the following primary antibodies overnight at 4˚C: Vinculin mouse mAb (1:50,000; cat. no. 66305-1-Ig; Proteintech Group, Inc.), CASP3 mouse mAb (1:2,000; cat. no. bsm-33284M; BIOSS), cleaved-CASP3 mouse mAb (1:2,000; cat. no. bsm-33199M; BIOSS), CASP1 rabbit pAb (1:2,000; cat. no. 22915-1-AP; Proteintech Group, Inc.), cleaved-CASP1 rabbit pAb (1:3,000; cat. no. PA5-77886; Thermo Fisher Scientific, Inc.), phospho-(p)MLKL rabbit pAb (1:2,000; cat. no. PA5-105677; Thermo Fisher Scientific, Inc.), total-(t)MLKL mouse mAb (1:50,000; cat. no. 66675-1-Ig; Proteintech Group, Inc.) and tRIPK3 rabbit pAb (1:10,000; cat. no. 29080-1-AP; Proteintech Group, Inc.). Membranes were incubated with the following secondary antibodies at room temperature for 2 h: Goat anti-mouse IgG HRP (1:4,000; cat. no. M21001L; Abmart, Inc.) and goat anti-rabbit IgG HRP (1:4,000; cat. no. M21002L; Abmart, Inc.). After visualization with an ECL detection kit (cat. no. 34580; Thermo Fisher Scientific, Inc.), images of membranes were captured using the GelDoc Go Gel Imaging System (Bio-Rad Laboratories, Inc.), and band intensities were semi-quantified using ImageJ 1.0 software (National Institutes of Health).

Reverse transcription-quantitative PCR (RT-qPCR) assay for TFRC and hub genes. Total RNA was extracted from BCPAP and K1 cells using TRIzol™ lysis buffer (cat. no. 15596018CN; Invitrogen™; Thermo Fisher Scientific, Inc.) and chloroform, followed by RNA concentration measurement using a NanoDrop™ 8000 Spectrophotometer (cat. no. ND-8000-GL; Thermo Fisher Scientific, Inc.). Reverse transcription of RNA and amplification of the target gene were performed using the FastKing RT Kit (cat. no. KR116; Tiangen Biotech Co., Ltd.) and Taq Pro Universal SYBR qPCR Master Kit (cat. no. Q712; Vazyme Biotech Co., Ltd.) on a 7500 PCR System (Thermo Fisher Scientific, Inc.). The conditions for reverse transcription were as follows: Incubation at 42˚C for 15 min, followed by heating at 95˚C for 3 min. The thermal cycling conditions for qPCR were as follows: Denaturation at 95˚C for 10 min, followed by annealing and extension at 95˚C for 15 sec and at 60˚C for 30 sec, with 45 cycles. The relative expression level of the target gene relative to GAPDH is calculated using the $2^{-\Delta\Delta Cq}$ method (33). The following primer sequences were used: 5'-TTGCCCTCAACGACCACTTT-3' [GAPDH-forward (F)]; 5'-TGGTCCAGGGGTCTTACTCC-3' [GAPDH-reverse (R)]; 5'-ATCTTGCGTTGTATGTTG-3' (TFRC-F); 5'-AGT CTACCGTTCTTATCAA-3' (TFRC-R); 5'-TCTACCTCT GTGATAACCT-3' (CD34-F); 5'-TGAACACTGTGCTGA TTA-3' (CD34-R); 5'-GATGATGTCTTCCTTAGTGTT-3' [lactate dehydrogenase A (LDHA)-F]; 5'-AGTCAGAGTCAC CTTCAC-3' (LDHA-R); 5'-GAAGAACTGGCGGCTTAA-3' [low-density lipoprotein receptor (LDLR)-F]; 5'-CCTCAT CCTCTGTGGTCT-3' (LDLR-R); 5'-TAAGACAATAGAGGT ATTCTG-3' [adaptor related protein complex 1 subunit μ 2 (AP1M2-F]; 5'-GTAGACGATGACAAAGTT-3' (AP1M2-R); 5'-CAGAATGATGATATTGGAAGTAGA-3' [diaphanous related formin 3 (DIAPH3)-F]; 5'-CAGGTTCACATAAGT TGCTAT-3' (DIAPH3-R); 5'-AGATGCTGCCAATAACTA TG-3' [tubulin α 1b (TUBA1B)-F]; 5'-AATTCGGTCCAACAC AAG-3' (TUBA1B-R); 5'-AACAACATTCGTAACTCTC-3' [citron ρ-interacting serine/threonine kinase (CIT)-F]; 5'-TTC TTCTCTGGTTCATCA-3' (CIT-R); 5'-CAACCTCGTAGA CTCCTA-3' [dynamin 3 (DNM3)-F]; 5'-TCCTCTGAAGAA TACAACTG-3' (DNM3-R); 5'-CGAAGAGGAATTGAGAAC TACTAT-3' [tetraspanin 15 (TSPAN15)-F]; 5'-GCCACAGCA CTTGAACTT-3' (TSPAN15-R); 5'-GATTACTATGGTCAC

TTG-3' [DEP domain containing 1B (DEPDC1B)-F]; 5'-CAT CATCCTCATCAATAG-3' (DEPDC1B-R); 5'-GACCACTAC CTAACTCAG-3' [IQ motif containing GTPase activating protein 3 (IQGAP3)-F]; 5'-GCATCATCAACAACTTCT A-3' (IQGAP3-R); 5'-AACAACAACTGGAACTTCAA-3' (CD24-F); 5'-CTTGGTGGTGGCATTAGT-3' (CD24-R); 5'-ATTAACCACTATCACCAT-3' [phosphoinositide-3-kinase regulatory subunit 3 (PIK3R3)-F]; and 5'-TATTCTTCATAC AGCCTAT-3' (PIK3R3-R).

TFRC-related mRNA-seq and bioinformatics analysis. Shanghai OE Biotech Co., Ltd performed sequencing of K1 cells from the KD-NC and KD-TFRC groups, including total RNA extraction, quality control, library construction, mRNA-seq on a sequencing platform (NovaSeq 6000; Illumina, Inc.) and subsequent bioinformatics analysis. Total RNA was extracted using the TRIzol reagent (15596026CN; Thermo Fisher Scientific, Inc.). RNA purity and quantification were evaluated using a spectrophotometer (NanoDrop 2000; Thermo Fisher Scientific, Inc.). RNA integrity was assessed using a Bioanalyzer (Agilent 2100; Agilent, Inc.). The libraries were then constructed using the VAHTS Universal V6 RNA-seq Library Prep Kit (NR616; Vazyme Biotech Co., Ltd.). The libraries were sequenced on a Novaseq 6000 sequencing platform and 150 bp paired-end reads were generated. For quality control, RseQC (v4.0.0) (34), fastp (v0.20.1) (35), hisat2 (v2.1.0) (36) and htseq-count (v0.11.2) (37) were applied to perform RNA integrity assessment, raw read quality filtering, base-level quality control, genome alignment and gene quantification, respectively. A total of 41.70 G clean data was generated from six K1 cell samples, with Q30 base range from 93.99-94.24%. Clean reads were mapped to the GRCh38.p13 reference genome with alignment rates of 97.81-98.13%. For downstream analysis, DESeq2 (v1.22.2) (38) was used to identify TFRC-associated differentially expressed (DE)-mRNAs; clusterProfiler (v4.4.4) (28) for GO, KEGG and gene set enrichment analysis (GSEA) enrichment analyses; ggplot (v3.3.6) (39) for data visualization; and the Network Analysis and MCODE (31) apps within Cytoscape software (v3.7.2) for PPI network construction and analysis. The shared genes between the ZBP1-related and the AIM2-related coding genes were obtained using the jvenn Web (https://jvenn.toulouse.inra.fr/app/example.html).

Statistical analyses. All data were replicated at least three times, and GraphPad Prism 9.0.0 software (Dotmatics) was used for statistical analyses, including Student's t-test or Mann-Whitney test and one-way ANOVA followed by Tukey's highly-significant differences post-hoc test or the Kruskal-Wallis test followed by Dunn's post-hoc test, as well as data visualization. Data were expressed as mean ± standard deviation. Pearson correlation analysis was used to identify coding genes associated with ZBP1 and AIM2 expression in the TCGA-THCA dataset. $P<0.05$ was considered to indicate a statistically significant difference.

Results

Identification and enrichment analysis of ZBP1- and AIM2-related coding genes. ZBP1 and AIM2 are well-established sensors of PANoptosis (7-11). To identify potential regulators of this process in TC, the present study analyzed protein-coding genes correlated with ZBP-1 and AIM2 expression in the TCGA-THCA cohort. A total of 729 and 1,568 genes were demonstrated to be significantly correlated with ZBP1 and AIM2 expression, respectively (P.adj <0.05; Fig. 1A). Venn diagram analysis revealed that there were 315 shared genes, including leucine aminopeptidase 3, CASP10, integrin subunit α L, 5'-nucleotidase cytosolic IIIA (*NT5C3A*) and *TFRC* (Fig. 1B). Functional enrichment analysis indicated that these genes were enriched in membrane- and vesicle-associated proteins, and were associated with 'leukocyte mediated immunity', 'response to tumor necrosis factor', 'extrinsic apoptotic signaling pathway', 'immune receptor activity' and 'tumor necrosis factor' (Fig. 1C). They were also enriched in pathways associated with 'natural killer cell mediated cytotoxicity', 'cytokine-cytokine receptor interaction', 'cell adhesion molecules', 'autoimmune thyroid disease', 'apoptosis' and 'necroptosis' (Fig. 1D). Collectively, these findings suggest that, in TC, coding genes associated with ZBP1 and AIM2 expression are primarily involved in immunity processes, apoptosis, necroptosis and cytokine-cytokine receptor interaction.

TFRC is associated with the prognosis of TC. To further identify hub genes associated with ZBP-1 and AIM2 expression in TC, a PPI network of 315 coding genes was constructed. This network contained 178 genes (nodes) and 608 relationship pairs (edges), using a minimum required interaction score of 0.9 in the STRING database (Fig. 2A). Network analysis revealed that the top five genes ranked by edge count were CD8A, interferon γ (*IFNG*), interferon induced protein 44, signal transducer and activator of transcription 1 (*STAT1*) and interferon-induced 15 KDa protein (*ISG15*), whereas the top five ranked by indegree were *STAT1*, radical S-adenosyl methionine domain containing 2, ubiquitin specific peptidase 18, *ISG15* and *IFNG*. To identify the key sub-networks, MCODE analysis was performed, and 10 clusters (clustering score ≥3) were detected (Fig. 2B). The sub-network with the highest clustering score (14.267) contained 16 genes (nodes) and 107 relationship pairs (edges), and was enriched in biological processes such as inflammatory response, apoptosis, oxidative stress and immune response, as well as pathways such as Toll-like receptor, retinoic acid-inducible gene-I-like receptor and cytosolic DNA-sensing. Moreover, the present study screened the genes associated with TC prognosis in this PPI network (178 genes/nodes). Univariate Cox analysis suggested that 15 coding genes were significantly associated with the prognosis of patients with TC. Furthermore, multivariate Cox analysis identified two independent risk factors, including TFRC and NT5C3A (Table I). Log-rank analysis demonstrated that low TFRC expression and high NT5C3A expression predicted reduced overall survival in patients with TC within 5,000 days (Fig. 2C). Consistently, TCGA-THCA expression data revealed that TFRC was downregulated and NT5C3A upregulated in TC tissues, compared with in normal tissues (Fig. 2D). Notably, the expression of TFRC and NT5C3A correlated positively with ZBP-1 and AIM2 (Fig. 1A). Although NT5C3A also demonstrated significant association with patient survival, the present study subsequently focused on TFRC due to its

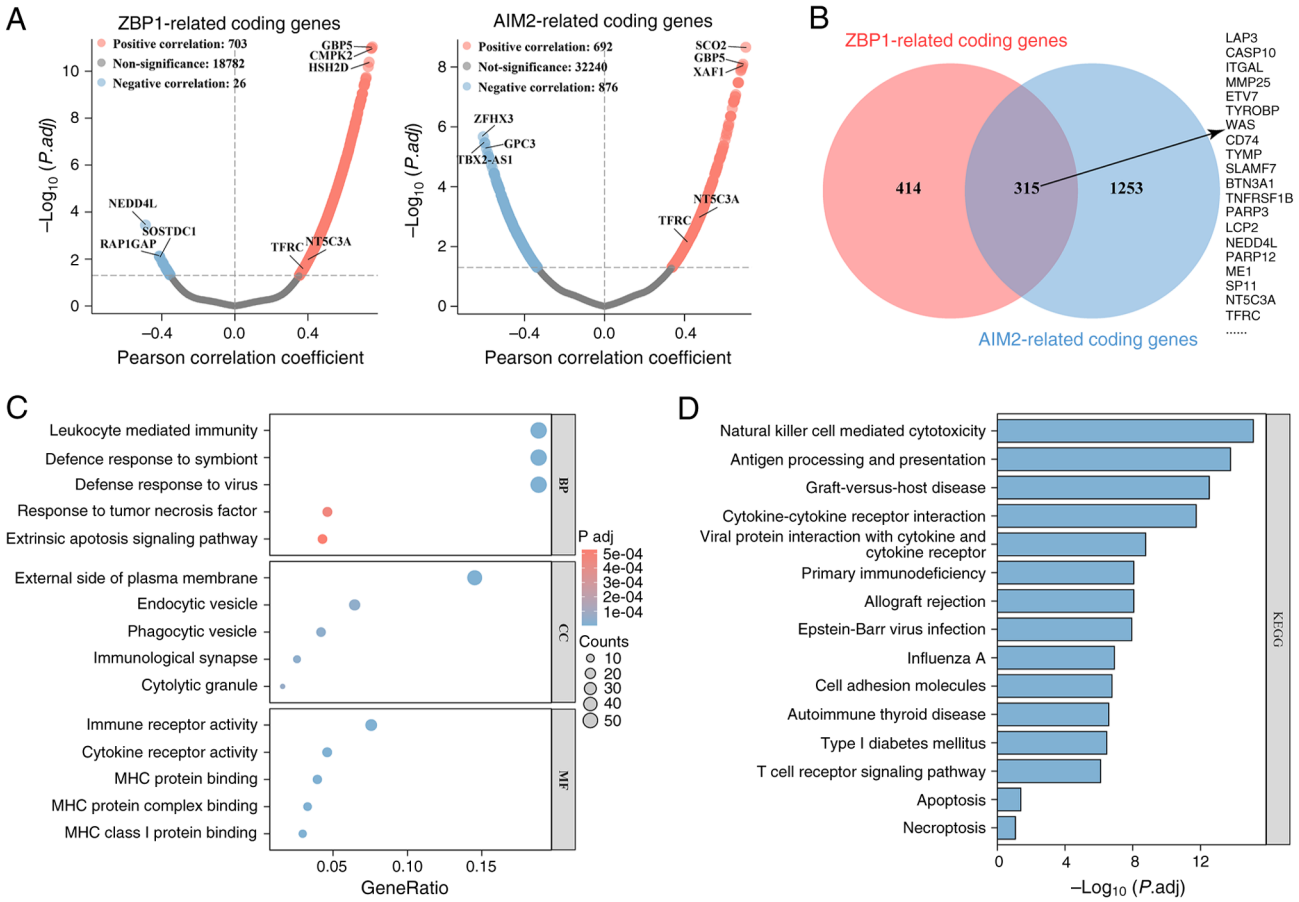

Figure 1. Identification and enrichment analysis of ZBP1- and AIM2-related coding genes. (A) Coding genes associated with ZBP1 and AIM2 expression in The Cancer Genome Atlas-Thyroid Cancer cohort were identified using Person correlation analysis. The volcano plots exhibit the results, with blue and red dots representing genes negatively and positively correlated with ZBP1 or AIM2, respectively. (B) Overlap and union of ZBP1- and AIM2-related coding genes, visualized using the jvenn Web (https://jvenn.toulouse.inra.fr/app/example.html). (C) Gene Ontology enrichment analysis of ZBP1- and AIM2-associated coding genes. The bubble plot presents the top five terms for BP, CC and MF. (D) KEGG pathway enrichment analysis of ZBP1- and AIM2-related coding genes. The bar chart depicts the top 15 pathways ranked by-$\log_{10}$(P.adj). ZBP1, Z-DNA-binding protein 1; AIM2, absent in melanoma 2; BP, biological process; CC, cellular component; MF, molecular function; KEGG, Kyoto Encyclopedia of Genes and Genomes.

established evidence across multiple cell death pathways, indicating greater potential for mechanism exploration. For experimental validation, TFRC expression was reduced in TC cell lines (TPC-1, K1 and BCPAP), with the lowest expression observed in BCPAP cells (Fig. 2E), consistent with TCGA-THCA profiles. Collectively, these findings suggest that TFRC functions as a prognostic factor and a potential regulator of PANoptosis in TC.

TFRC facilitates PANoptosis for TC. To further investigate the role of TFRC in regulating PANoptosis in TC cells *in vitro*, the present study performed *in vitro* functional experiments. TFRC was overexpressed in BCPAP cells, which exhibit relatively low endogenous TFRC expression, and silenced in K1 cells, which express higher TFRC levels. RT-qPCR demonstrated that PGMLV-CMV-MCS-EF1-ZsGreen1-T2A-Puro and shRNA effectively regulated the level of *TFRC* mRNA in BCPAP and K1 cells (Fig. 3A and B). Calcein-AM/PI staining revealed a marked increase in PI^+ BCPAP cells in the OV-TFRC group, whereas a notable decrease in PI^+ K1 cells was observed in the KD-TFRC group, compared with their respective controls (Fig. 3C). These results indicate that TFRC facilitates TC cell death.

To further distinguish the mode of cell death, YO-PRO-1/PI staining was performed. Overexpression of TFRC notably increased the proportion of YO-PRO-1-positive cells (apoptosis/necroptosis) and PI-positive cells (necroptosis/pyroptosis) in BCPAP cells, whereas the opposite trend was observed following TFRC knockdown (Fig. 3D). These findings suggest that TFRC promotes multiple forms of regulated cell death, including pyroptosis, apoptosis and necroptosis, in TC cells. Consistent with these observations, western blot analysis revealed that, compared with in the OV-NC or KD-NC groups, the expression levels of cleaved-CASP1, CASP1, cleaved-CASP3, CASP3, pMLKL and tRIPK3 proteins were significantly augmented in BCPAP cells overexpressing TFRC, but reduced in K1 cells with TFRC knockdown (Fig. 3E). Collectively, these results indicate that overexpression of TFRC drives PANoptosis in TC cells.

Identification and enrichment analysis of TFRC-associated DE-mRNAs. To explore the potential mechanism underlying TFRC-associated PANoptosis in TC cells, mRNA-seq was performed on K1 cells from the KD-NC and KD-TFRC groups. The results demonstrated that mRNA expression profiles clustered tightly within groups, but were clearly

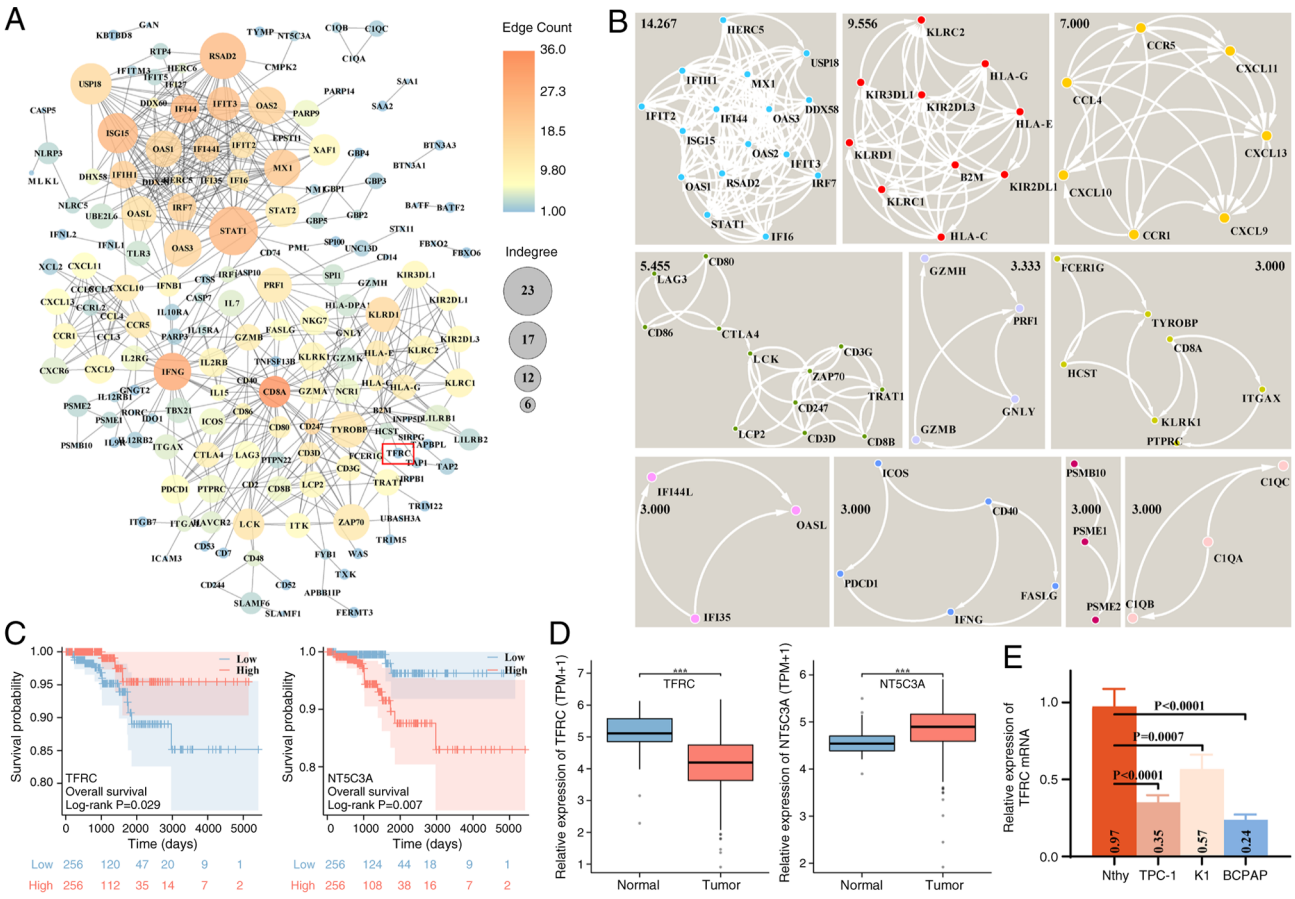

Figure 2. PPI network construction of ZBP1- and AIM2-related coding genes and prognostic analysis of hub genes in TC. (A) PPI networks of ZBP1 and AIM2 co-associated genes, constructed using the STRING database and visualized using Cytoscape software. Node color and size indicate edge counts and indegree, respectively. (B) Sub-networks within the PPI network were identified using the MCODE app in Cytoscape software. Black numbers denote the clustering scores of each sub-network. (C) Prognostic significance of TFRC and NT5C3A expression in patients with TC, evaluated using log-rank analysis in the TCGA-THCA cohort. (D) Differential expression of TFRC and NT5C3A in the TCGA-THCA cohort. (E) Relative TFRC mRNA expression in Nthy and TC cells (TPC-1, K1 and BCPAP), assessed using reverse transcription-quantitative PCR assay. ***P<0.001. PPI, protein-protein interaction; ZBP1, Z-DNA-binding protein 1; AIM2, absent in melanoma 2; TC, thyroid cancer; TFRC, transferrin receptor; NT5C3A, 5'-nucleotidase cytosolic IIIA; TCGA-THCA, The Cancer Genome Atlas-Thryoid Cancer; Nthy, normal human thyroid epithelial; TPM, transcripts per million.

separated between groups, indicating distinct gene expression patterns (Fig. 4A). Compared with the KD-NC group, the KD-TFRC group exhibited 360 significantly downregulated DE-mRNAs and 468 significantly upregulated DE-mRNAs (Fig. 4B). Radar plots highlighted the top 30 DE-mRNAs ranked by $|\log_2$FoldChange (FC)|, with inhibitor of DNA binding 1, NADPH oxidase 5, regulator of G protein signaling 4, collagen type VIII α1 chain and secreted phosphoprotein 1 among the most upregulated, and deleted in azoospermia like, early growth response 1, leucine rich repeat containing 15, hephaestin like 1 and dishevelled binding antagonist of β catenin 1 among the most downregulated (Fig. 4C). GO enrichment analysis indicated that TFRC-associated DE-mRNAs were predominantly localized to the extracellular matrix and enriched in processes such as 'pyroptosis', 'negative regulation of apoptotic process', 'immune response' and 'cellular response to tumor necrosis factor' (Fig. 4D). KEGG enrichment analysis further demonstrated enrichment in 'cell cycle', 'TNF signaling pathway', 'ECM-receptor interaction', 'cytokine-cytokine receptor interaction' and 'IL-17 signaling pathway' (Fig. 4E). Consistently, GSEA analysis revealed that knockdown of TFRC was associated with cell proliferation, unsaturated fatty acid biosynthesis and pyrimidine metabolism, whilst suppressing immune-related processes (Fig. 5). Collectively, these findings suggest that TFRC-associated DE-mRNAs are mainly involved in regulating the cell cycle, apoptosis, necrotic apoptosis, pyroptosis, angiogenesis, oxidative stress and immunity, thereby reflecting the molecular mechanisms of TFRC-mediated PANoptosis in TC cells.

Identification of hub genes for TFRC-associated DE-mRNAs. The present study further constructed a PPI network comprising 828 TFRC expression-associated DE-mRNAs. This PPI network consisted of 122 genes and 535 interrelationship pairs, with the top five hub genes ranked by degree centrality being *CDC20*, *kinesin family member 11*, *polo like kinase 1*, *budding uninhibited by benzimidazoles 1* (yeast homolog) and *CDK1* (Fig. 6A). MCODE analysis further identified six sub-networks (clustering scores ≥3) (Fig. 6B). The most notable sub-network, with a clustering score of 15.789, contained 20 genes and 150 interaction pairs, including *assembly factor for spindle microtubule*, *aurora kinase B*, *cell division cycle-associated protein 1* and *centromere protein f* and *kinesin family member 2C*, which are primarily involved in regulating the cell cycle and

Table I. Cox regression analysis of Z-DNA-binding protein 1 and absent in melanoma 2 expression-related coding genes in thyroid cancer.

Gene (low vs. high expression)	Univariate analysis		Multivariate analysis	
	HR (95% CI)	P-value	HR (95% CI)	P-value
ISG15	0.305 (0.098-0.949)	0.040	1.339 (0.249-7.211)	0.734
IL2RB	0.208 (0.059-0.732)	0.014	0.521 (0.077-3.542)	0.505
PARP9	0.318 (0.102-0.988)	0.048	0.723 (0.136-3.839)	0.704
IFIT2	0.320 (0.103-0.992)	0.048	1.480 (0.305-7.176)	0.626
CXCL10	0.304 (0.098-0.942)	0.039	1.062 (0.195-5.765)	0.945
CD8B	0.318 (0.103-0.987)	0.047	0.798 (0.193-3.300)	0.755
HLA-G	0.215 (0.061-0.755)	0.016	0.289 (0.055-1.525)	0.143
PSME2	0.246 (0.070-0.866)	0.029	2.505 (0.350-17.920)	0.360
PSME1	0.073 (0.010-0.554)	0.011	0.119 (0.010-1.416)	0.092
RTP4	0.144 (0.033-0.636)	0.011	0.434 (0.063-3.006)	0.398
GBP2	0.279 (0.089-0.869)	0.028	0.701 (0.147-3.350)	0.656
HERC6	0.280 (0.090-0.872)	0.028	1.246 (0.255-6.082)	0.786
TFRC	1.270 (1.077-1.949)	0.041	1.146 (1.035-1.618)	0.019
NT5C3A	4.773 (1.359-16.759)	0.015	7.464 (1.387-40.175)	0.009
PARP14	0.206 (0.059-0.724)	0.014	0.466 (0.078-2.781)	0.402

HR, hazard ratio; CI, confidence interval; ISG15, interferon-induced 15 KDa protein; IL2RB, interleukin 2 receptor subunit β; PARP, poly(ADP-Ribose) polymerase; IFIT2, interferon induced protein with tetratricopeptide repeats 2; CXCL10, C-X-C motif chemokine ligand 10; NCR1, natural cytotoxicity triggering receptor 1; HLA-G, major histocompatibility complex, class I, G; PSME, proteasome activator; RTP4, receptor transporter protein 4; GBP2, guanylate binding protein 2; HERC6, HECT and RLD domain containing E3 ubiquitin protein ligase family member 6; TFRC, transferrin receptor; NT5C3A, 5'-nucleotidase cytosolic IIIA.

immunity (40-44). Notably, the STRING database predicted potential interactions between TFRC and 13 genes, namely *CD34*, *LDHA*, *LDLR*, *AP1M2*, *DIAPH3*, *TUBA1B*, *CIT*, *DNM3*, *TSPAN15*, *DEPDC1B*, *IQGAP3*, *CD24* and *PIK3R3* (Fig. 6C). Consistently, mRNA expression profile of K1 cells revealed a strong positive correlation between TFRC expression and the mRNAs levels of these genes (Fig. 6D). RT-qPCR revealed that TFRC knockdown led to significant reductions in the mRNA levels of *PIK3R3*, *LDLR*, *LDHA*, *IQGAP3*, *CIT*, *CD34*, *DNM3*, *AP1M2* and *CD24* in K1 cells, compared with controls (Fig. 6E), which was consistent with the results of the correlation analysis (Fig. 6D). Collectively, these findings suggest that the pro-PANoptotic role of TFRC in TC may be mediated, at least in part, through its association with these 13 genes.

Discussion

The present study identified 315 coding genes associated with ZBP-1 and AIM2 expression, among which TFRC and NT5C3A emerged as significantly associated with the prognosis of patients with TC. Although NT5C3A also demonstrated a significant association with patient survival and represents a promising candidate for future studies, the present study subsequently focused on TFRC due to its established evidence across multiple cell death pathways, indicating greater potential for mechanism exploration in the context of PANoptosis. Notably, TFRC mRNA was expressed at low levels in TC cells (TPC-1, K1 and BCPAP) yet facilitated PANoptosis process. Notably, in TFRC-related experiments, inducers were not employed to trigger PANoptosis in TC cells. Since Malireddi *et al* (45) first proposed PANoptosis, PANoptosis-related studies have not utilized induction agents, to the best of our knowledge (46-53). This may be due to the lack of specific PANoptosis inducers. Therefore, in subsequent experiments in the present study, an inducer for treatment was not used.

TFRC has previously been implicated in the regulation of cell death. Earlier studies reported that TFRC primarily promotes ferroptosis, as reported in endometrial cancer (54), sepsis-associated encephalopathy (55) and colorectal cancer (21). In addition, TFRC has been reported to regulate apoptosis in nasopharyngeal carcinoma cells (56), pyroptosis in sheep hepatocytes and hepatocytes (57), and necroptosis in placenta (58). However, its role in TC has remained unexplored, despite bioinformatics analyses suggesting TFRC as a ferroptosis-related feature predictive of TC prognosis (17,18). Therefore, the present study refined the understanding of TFRC-mediated cell death and demonstrated, for the first time to the best of our knowledge, its involvement in PANoptosis process in TC.

Furthermore, to elucidate the molecular mechanism underlying TFRC regulation of PANoptosis, the present study performed mRNA-seq and identified 828 TFRC-associated DE-mRNAs enriched in biological processes and pathways including cell cycle, apoptosis, necrotic apoptosis, pyroptosis,

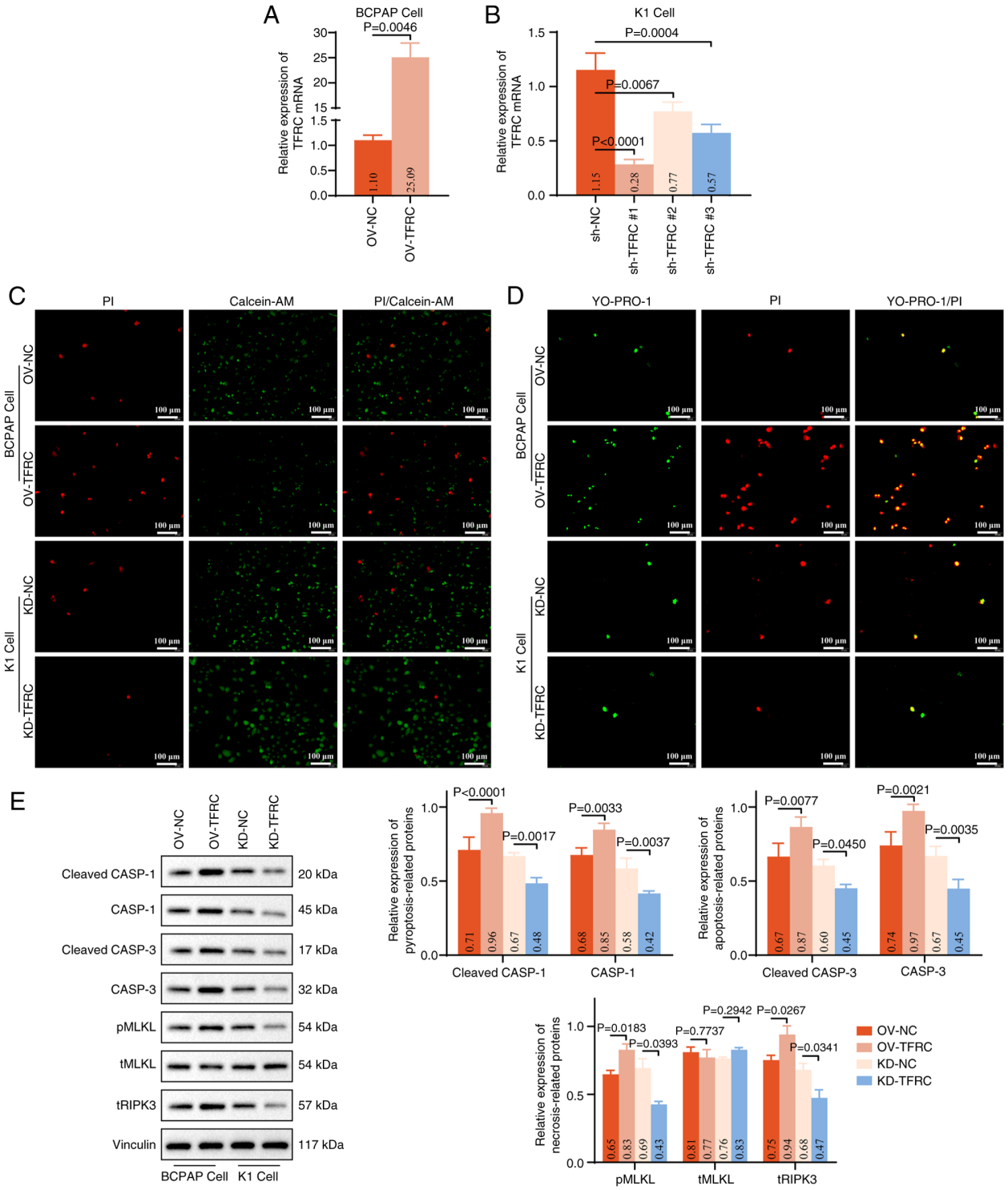

Figure 3. TFRC contributes to PANoptosis in TC cells. Effects of (A) PGMLV-CMV-MCS-EF1-ZsGreen1-T2A-Puro and (B) shRNA transfection on the expression of *TFRC* mRNA in BCPAP and K1 cells, assessed using reverse transcription-quantitative PCR assay. (C) PI/Calcein-AM staining was performed to assess the effect of TFRC on cell death in BCPAP (OV-NC and OV-TFRC groups) and K1 (KD-NC and KD-TFRC groups) cells. PI (red) and Calcein-AM (green) label dead and viable cells, respectively. (D) YO-PRO-1/PI staining was performed to evaluate pyroptosis, apoptosis and necroptosis in BCPAP and K1 cells following exogenous modulation of TFRC expression. YO-PRO-1 (green) indicates apoptotic or necroptotic cells, whereas PI (red) labels necroptotic or pyroptotic cells. (E) Western blot analysis of markers associated with pyroptosis (cleaved-CASP1/CASP1), apoptosis (cleaved-CASP3/CASP3) and necroptosis (pMLKL/tMLKL and tRIPK3), with corresponding quantitative analyses. TFRC, transferrin receptor; sh, short hairpin; OV, overexpression; NC, negative control; KD, knockdown; CASP; caspase; MLKL, mixed lineage kinase domain like pseudokinase; pMLKL, phospho-MLKL; tMLKL, total-MLKL; tRIPK3, total receptor interacting serine/threonine kinase 3.

angiogenesis, oxidative stress and immunity. Among these, 13 DE-mRNAs (*CD34*, *LDHA*, *LDLR*, *AP1M2*, *DIAPH3*, *TUBA1B*, *CIT*, *DNM3*, *TSPAN15*, *DEPDC1B*, *IQGAP3*, *CD24* and *PIK3R3*) were predicted to interact with TFRC and displayed a positive correlation with its expression in TC. Notably, these DE-mRNAs are implicated in the progression

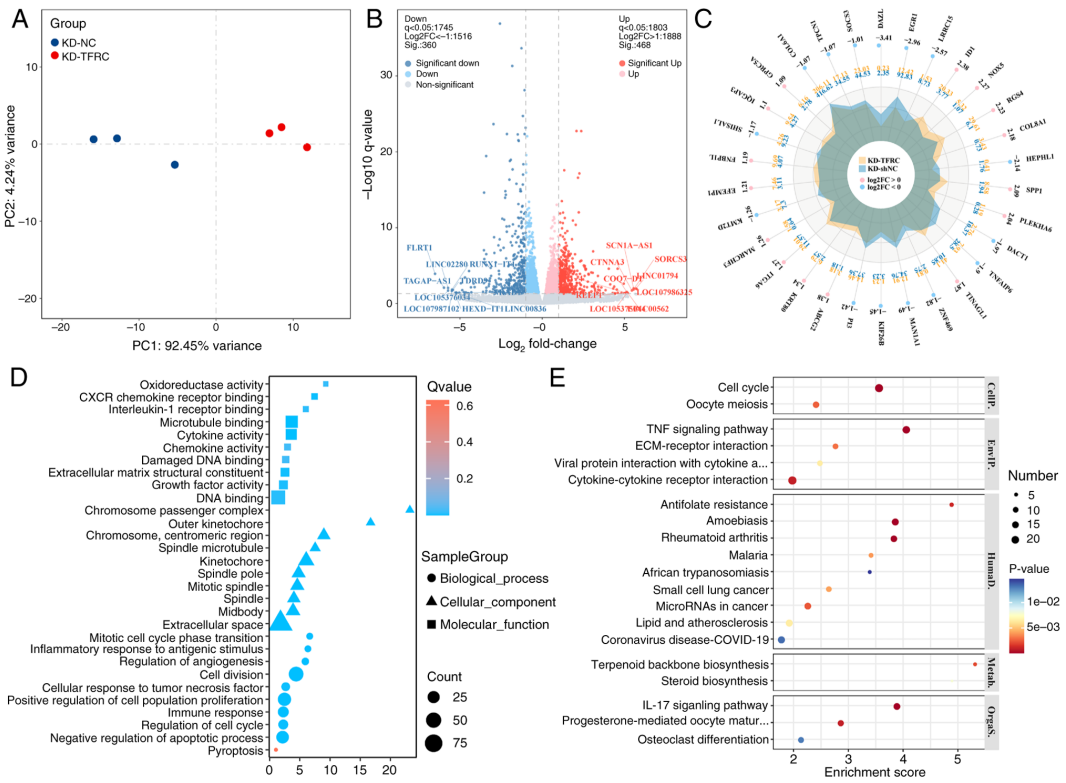

Figure 4. Identification and enrichment analysis of TFRC-associated DE-mRNAs in thyroid cancer. (A) Principal component analysis of mRNA expression profiles in K1 cells (KD-NC and KD-TFRC groups). Blue and red dots represent cell samples of KD-NC and KD-TFRC groups, respectively. (B) Differential expression analysis of mRNA expression profiles between the KD-NC and KD-TFRC groups. The volcano plot illustrates the distribution and regulation of TFRC-associated DE-mRNAs. (C) Radar plot displaying the top 30 DE-mRNAs ranked by $|\log_2 FC|$ in K1 cells. Functional annotation of TFRC-associated DE-mRNAs: (D) Gene Ontology and (E) and Kyoto Encyclopedia of Genes and Genomes pathway enrichment analyses, with bubble plots highlighting the most significantly enriched terms. TFRC, transferrin receptor; DE-mRNAs, differentially expressed mRNAs; KD, knockdown; NC, negative control; FC, fold change.

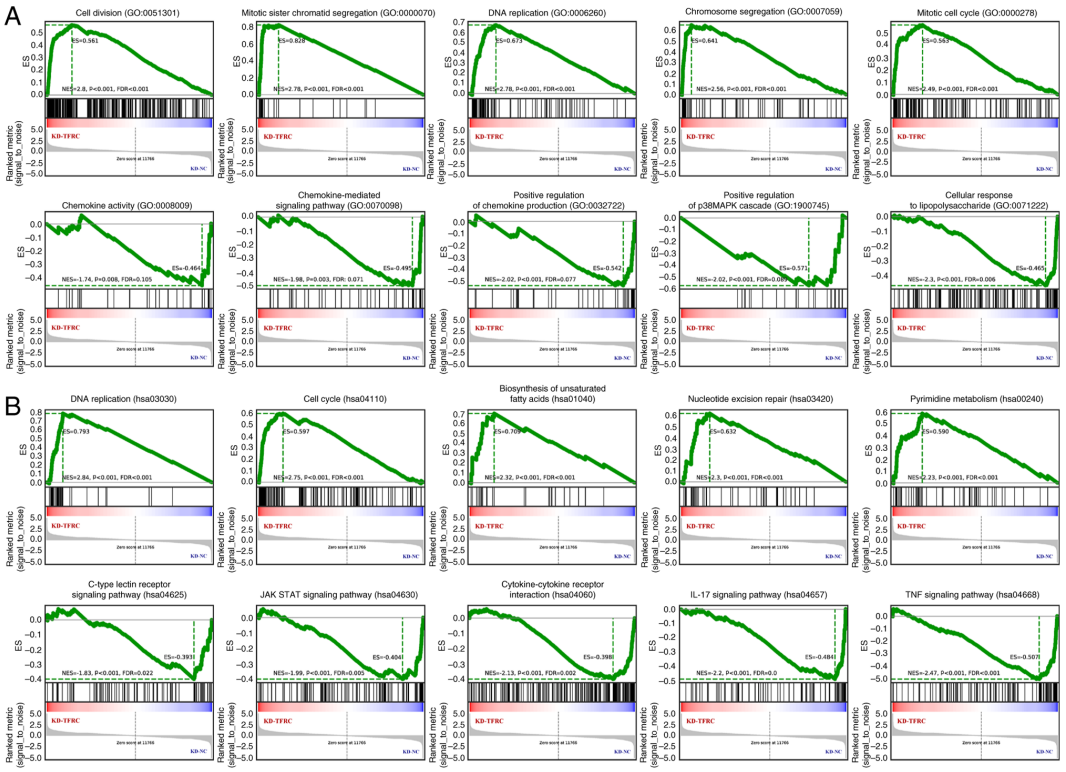

Figure 5. GSEA of TFRC-associated differentially expressed mRNAs in thyroid cancer. (A) GO and (B) Kyoto Encyclopedia of Genes and Genomes terms associated with GSEA results. GSEA, gene set enrichment analysis; TFRC, transferrin receptor; GO, Gene Ontology; KD, knockdown; NES, normalized enrichment score; FDR, false discovery rate; NC, negative control.

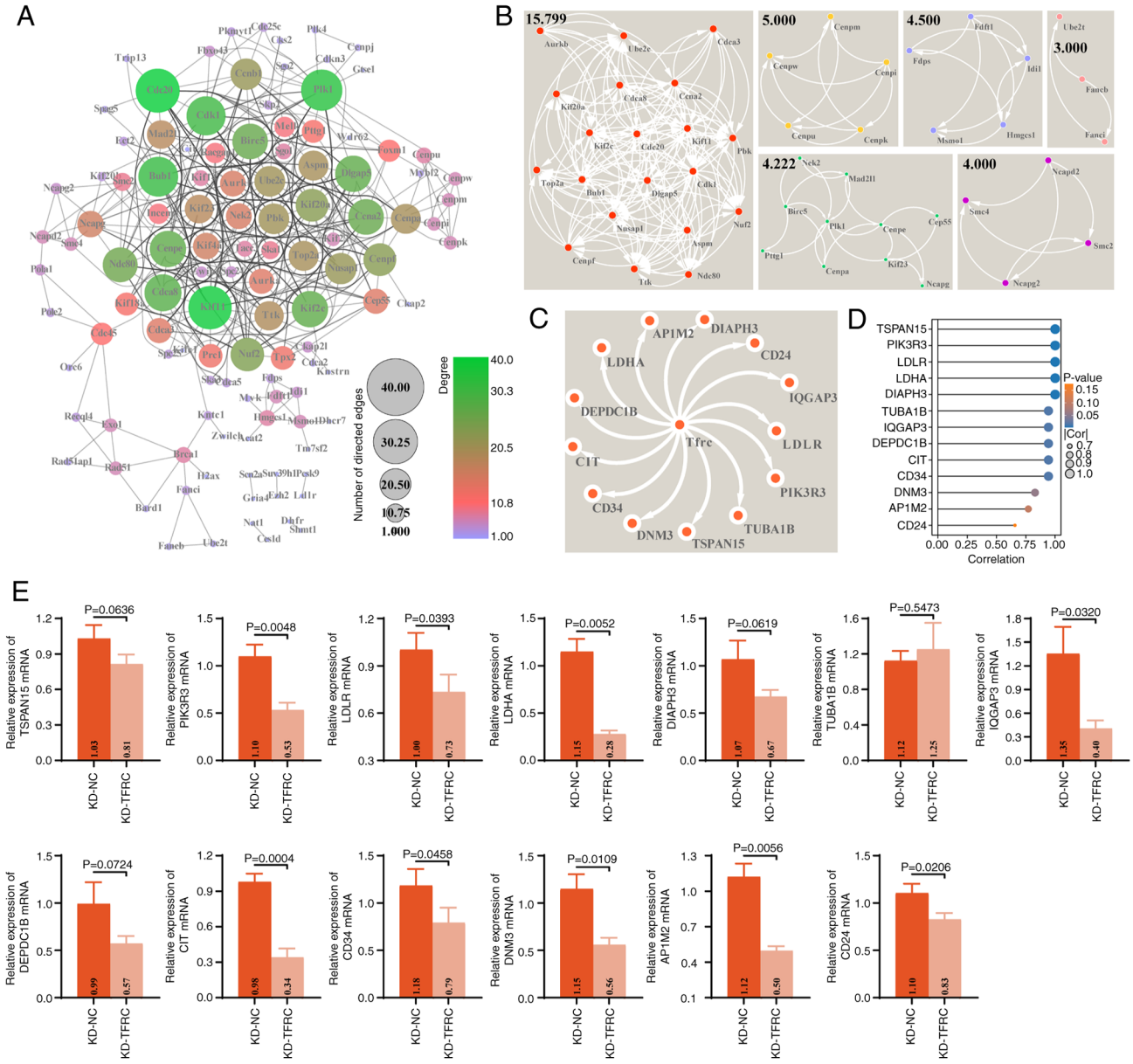

Figure 6. PPI network of TFRC-associated DE-mRNAs in thyroid cancer. (A) PPI network of TFRC-associated DE-mRNAs constructed and visualized in Cytoscape software. Node color and size represent degree and indegree, respectively. (B) Sub-networks within the PPI network identified using the MCODE app in Cytoscape software. (C) Predicted TFRC-interacting genes obtained from the STRING database (minimum required interaction score, 0.4). (D) Lollipop plot showing the correlation between TFRC and the expression of *CD34*, *LDHA*, *LDLR*, *AP1M2*, *DIAPH3*, *TUBA1B*, *CIT*, *DNM3*, *TSPAN15*, *DEPDC1B*, *IQGAP3*, *CD24* and *PIK3R3* in the mRNA expression profiles of K1 cells (KD-NC and KD-TFRC groups). (E) Effects of TFRC knockdown on the mRNA expressions of *CD34*, *LDHA*, *LDLR*, *AP1M2*, *DIAPH3*, *TUBA1B*, *CIT*, *DNM3*, *TSPAN15*, *DEPDC1B*, *IQGAP3*, *CD24* and *PIK3R3* in K1 cells, assessed using reverse transcription-quantitative PCR. PPI, protein-protein interaction; DE-mRNAs, differentially expressed mRNAs; TFRC, transferrin receptor; KD, knockdown; NC, negative control; LDHA, lactate dehydrogenase A; LDLR, low-density lipoprotein receptor; AP1M2, adaptor related protein complex 1 subunit μ 2; DIAPH3, diaphanous related formin 3; TUBA1B, tubulin α 1b; CIT, citron ρ-interacting serine/threonine kinase; DNM3, dynamin 3; TSPAN15, tetraspanin 15; DEPDC1B, DEP domain containing 1B; IQGAP3, IQ motif containing GTPase activating protein 3; PIK3R3, phosphoinositide-3-kinase regulatory subunit 3.

of TC process and functionally associated with apoptosis, necroptosis and pyroptosis. CD34, LDHA, and LDLR are well-established markers of angiogenesis, glycolysis and cholesterol metabolism, respectively, in malignant tumors, and have also been associated with apoptotic and pyroptotic pathways (59-61). Moreover, DNM3 has been reported to be markedly downregulated in TCs, where it facilitates tumor cell death (62). DIAPH3, DEPDC1B, CD24 and PIK3R3 have each been implicated in the regulation of tumor cell death (63,64). Notably, the present study demonstrated that TFRC expression was positively correlated with these DE-mRNAs, and its knockdown effectively reduced the levels of PIK3R3, LDLR, LDHA, IQGAP3, CIT, CD34, DNM3, AP1M2h and CD24. However, although the present study identified 13 TFRC-interacting DE-mRNAs, none have been directly established as core regulators of PANoptosis in existing literature. Instead, these genes are primarily associated with distinct biological processes such as angiogenesis (*CD34*), cholesterol metabolism (*LDLR*) and cytoskeletal organization (*DIAPH3*). Several, including *DIAPH3*, *DEPDC1B*, *CD24* and *PIK3R3*, have been associated

with apoptosis or other forms of regulated cell death, but not to the integrated PANoptosis pathway (59-64). This suggests that TFRC may orchestrate PANoptosis, not through direct engagement of these DE-mRNAs as PANoptosis-specific effectors, but by modulating broader networks involving immunity, metabolism and stress response.

Among these, the interaction between TFRC and LDHA may link glycolysis and lactylation modification to the PANoptosis process. LDHA is the key enzyme catalyzing the final step of glycolysis, converting pyruvate into lactate. This process provides efficient ATP for rapid tumor cell proliferation and supplies an abundant lactate pool for lactate modification (65,66). Previous study has reported that the PANoptosis process is mediated by glycolysis during radiotherapy for esophageal cancer (12). Simultaneously, lactylation modification induced by lactic acid accumulation regulates the PANoptosis process through multiple signaling cascades, including the Arg1/Mic10/voltage dependent anion channel 1 axis, the cold inducible RNA binding/toll like receptor 4/ZBP1/tripartite motif containing 32/RIPK3 axis and the proteasome 26S subunit, non-ATPase 14/pyruvate kinase M1/2/PINK1 axis (67-69). Notably, lactate efflux via monocarboxylate transporters acidifies the tumor microenvironment (TME), triggering damage-associated molecular patterns (DAMPs) that induce stress signals leading to inflammatory cell death in adjacent immune cells and cancer cells (70). Furthermore, lactylation activates downstream inflammatory cascades (TNF-α, IL-1β, IL-6 and IL-12) by regulating S100 and high mobility group box 1 in DAMPs (71,72). Notably, DAMP is one of the pathways that trigger PANoptosis (7-11). The present study revealed that the expression of TFRC and LDHA was positively associated during the PANoptosis process in TC, and TFRC knockdown inhibited LDHA expression in K1 cells. Therefore, we hypothesize that the interaction between TFRC and LDHA may accelerate glycolysis and lactate production. Further, accumulated lactic acid serves as a substrate to induce lactylation of DAMP-associated proteins, thereby regulating pro-inflammatory gene expression. Meanwhile, lactic acid triggers inflammatory death through stress signals in an acidic TME. These pathways together activate the PANoptosome complex, ultimately synergistically triggering PANoptosis. Therefore, the TFRC-LDHA-lactylation pathway may provide a novel mechanism linking tumor glycolysis to PANoptosis. Collectively, these findings suggest the occurrence of PANoptosis in TC may be an outcome of TFRC interactions with these DE-mRNAs.

Although the present study proposes a potential mechanism by which TFRC regulates PANoptosis in TC, the precise mode of action remains unclear and requires further validation. In particular, it is not yet known at which molecular level (protein, RNA or DNA) and through what mechanisms TFRC interacts with the identified DE-mRNAs. These issues warrant investigation using approaches such as chromatin immunoprecipitation, pull down, co-immunoprecipitation and RNA-binding protein immunoprecipitation. Moreover, the potential interactions of TFRC with the PANoptosis sensors, ZBP1 and AIM2, also require verification. Finally, the absence of *in vivo* experiments in the present study limits direct evidence for TFRC-mediated regulation of PANoptosis in TC. The findings suggest a potential association between TFRC and LDHA expression, which may indirectly implicate glycolytic and lactylation pathways in PANoptosis regulation. However, direct experimental validation of LDHA function and lactate metabolism remains to be investigated in future studies. Subsequently, experiments such as LDHA knockdown/overexpression, lactate measurement and histone lactylation detection need be performed to further verify whether this pathway is indeed involved in TFRC-mediated PANoptosis.

In conclusion, the present study provides the first evidence, to the best of our knowledge, that TFRC contributes to PANoptosis process in TC and delineates a potential regulatory pathway using mRNA-seq. The findings not only advance the understanding of PANoptosis in TC but also hold promise for informing future therapeutic strategies targeting this pathway. To exploit TFRC for TC treatment, several strategies could be considered to increase its expression or activity in tumor cells. Small molecule agonists or transcriptional activators that enhance TFRC expression could be developed. Additionally, nanoparticle-based delivery systems could be designed to deliver TFRC-expressing plasmids or mRNA directly into tumor cells, thereby restoring TFRC function and inducing PANoptosis. Future studies should focus on validating these strategies in preclinical models and ultimately in clinical trials to translate TFRC-based PANoptosis induction into a viable therapeutic option for patients with TC.

Acknowledgements

Not applicable.

Funding

The present study was supported by the Yunnan Provincial Health Commission 'Medical Leading Talents' Training Program (grant no. L-2018015) and Yunnan Province 'Ten Thousand People Plan' Special Medical Talents (grant no. 2019-35).

Availability of data and materials

The data generated in the present study may be found in the Gene Expression Omnibus under accession number GSE280138 (Secure Token: ctgxycgmjrazxob) or at the following URL: https://www.ncbi.nlm.nih.gov/geo/query/acc.cgi?acc=GSE280138. All other data generated in the present study may be requested from the corresponding author.

Authors' contributions

SM and ZM conceived and designed the experiments; SM, JS, HL, HY, YH and SY performed the experiments; SM and JS analyzed and interpreted the data; HL, HY, YH and SY sourced the reagents, materials and analysis tools; SM wrote original draft; and ZM, JS, HL, HY, YH and SY reviewed and edited the manuscript draft. SM, ZM, JS, HL, HY, YH and SY checked and confirmed the authenticity of all the raw data. All authors read and approved the final manuscript.

Ethics approval and consent to participate

Not applicable.

Patient consent for publication

Not applicable.

Competing interests

The authors declare that they have no competing interests.

References

1. Chen DW, Lang BHH, McLeod DSA, Newbold K and Haymart MR: Thyroid cancer. Lancet 401: 1531-1544, 2023.
2. Sung H, Ferlay J, Siegel RL, Laversanne M, Soerjomataram I, Jemal A and Bray F: Global cancer statistics 2020: GLOBOCAN estimates of incidence and mortality worldwide for 36 cancers in 185 countries. CA Cancer J Clin 71: 209-249, 2021.
3. Rahib L, Smith BD, Aizenberg R, Rosenzweig AB, Fleshman JM and Matrisian LM: Projecting cancer incidence and deaths to 2030: The unexpected burden of thyroid, liver, and pancreas cancers in the United States. Cancer Res 74: 2913-2921, 2014.
4. Zhang L, Feng Q, Wang J, Tan Z, Li Q and Ge M: Molecular basis and targeted therapy in thyroid cancer: Progress and opportunities. Biochim Biophys Acta Rev Cancer 1878: 188928, 2023.
5. Laha D, Nilubol N and Boufraqech M: New therapies for advanced thyroid cancer. Front Endocrinol (Lausanne) 11: 82, 2020.
6. Shen H, Zhu R, Liu Y, Hong Y, Ge J, Xuan J, Niu W, Yu X, Qin JJ and Li Q: Radioiodine-refractory differentiated thyroid cancer: Molecular mechanisms and therapeutic strategies for radioiodine resistance. Drug Resist Updat 72: 101013, 2024.
7. Pandian N and Kanneganti TD: PANoptosis: A unique innate immune inflammatory cell death modality. J Immunol 209: 1625-1633, 2022.
8. Samir P, Malireddi RKS and Kanneganti TD: The PANoptosome: A deadly protein complex driving pyroptosis, apoptosis, and necroptosis (PANoptosis). Front Cell Infect Microbiol 10: 238, 2020.
9. Karki R and Kanneganti TD: PANoptosome signaling and therapeutic implications in infection: Central role for ZBP1 to activate the inflammasome and PANoptosis. Curr Opin Immunol 83: 102348, 2023.
10. Nozaki K, Li L and Miao EA: Innate sensors trigger regulated cell death to combat intracellular infection. Annu Rev Immunol 40: 469-498, 2022.
11. Lee S, Karki R, Wang Y, Nguyen LN, Kalathur RC and Kanneganti TD: AIM2 forms a complex with pyrin and ZBP1 to drive PANoptosis and host defence. Nature 597: 415-419, 2021.
12. Liu LX, Heng JH, Deng DX, Zhao H, Zheng ZY, Liao LD, Lin W, Xu XE, Li EM and Xu LY: Sulconazole induces PANoptosis by triggering oxidative stress and inhibiting glycolysis to increase radiosensitivity in esophageal cancer. Mol Cell Proteomics 22: 100551, 2023.
13. Karki R, Sundaram B, Sharma BR, Lee S, Malireddi RKS, Nguyen LN, Christgen S, Zheng M, Wang Y, Samir P, *et al*: ADAR1 restricts ZBP1-mediated immune response and PANoptosis to promote tumorigenesis. Cell Rep 37: 109858, 2021.
14. Ren L, Yang Y, Li W, Zheng X, Liu J, Li S, Yang H, Zhang Y, Ge B, Zhang S, *et al*: CDK1 serves as a therapeutic target of adrenocortical carcinoma via regulating epithelial-mesenchymal transition, G2/M phase transition, and PANoptosis. J Transl Med 20: 444, 2022.
15. Cai Y, Chen X, Lu T, Fang X, Ding M, Yu Z, Hu S, Liu J, Zhou X and Wang X: Activation of STING by SAMHD1 deficiency promotes PANoptosis and enhances efficacy of PD-L1 blockade in diffuse Large B-cell lymphoma. Int J Biol Sci 19: 4627-4643, 2023.
16. Karbakhsh Ravari F, Ghasemi Gorji M and Rafiei A: From iron-driven cell death to clot formation: The emerging role of ferroptosis in thrombogenesis. Biomed Pharmacother 189: 118328, 2025.
17. Shi J, Wu P, Sheng L, Sun W and Zhang H: Ferroptosis-related gene signature predicts the prognosis of papillary thyroid carcinoma. Cancer Cell Int 21: 669, 2021.
18. Yang D, Wang J, Li C, Shi L and Zhang M: Ferroptosis-related gene model to predict overall survival of papillary thyroid carcinoma. Am J Otolaryngol 42: 103163, 2021.
19. Huang Y, Du J, Li D, He W, Liu Z, Liu L, Yang X, Cheng X, Chen R and Yang Y: LASS2 suppresses metastasis in multiple cancers by regulating the ferroptosis signalling pathway through interaction with TFRC. Cancer Cell Int 24: 87, 2024.
20. Zhou X, Nie M, Xin X, Hua T, Zhang J, Shi R, Dong K, Shu W, Yan B and Wang H: RAB17 promotes endometrial cancer progression by inhibiting TFRC-dependent ferroptosis. Cell Death Dis 15: 655, 2024.
21. Wang X, Zhou Y, Ning L, Chen J, Chen H and Li X: Knockdown of ANXA10 induces ferroptosis by inhibiting autophagy-mediated TFRC degradation in colorectal cancer. Cell Death Dis 14: 588, 2023.
22. Guo S, Chen Y, Xue X, Yang Y, Wang Y, Qiu S, Cui J, Zhang X, Ma L, Qiao Y and Wang J: TRIB2 desensitizes ferroptosis via βTrCP-mediated TFRC ubiquitiantion in liver cancer cells. Cell Death Discov 7: 196, 2021.
23. Lin Z, Zhong C, Shi M, Long Q, Jing L, Yu Y, Chou J, Chen M, Lan M and Long F: Circular RNA TFRC/SCD1 mRNA interaction regulates ferroptosis and metastasis in gastric cancer. Cell Death Dis 16: 436, 2025.
24. Wang WT, Duan ZW, Xing TY, Hua W, Du KX, Shang CY, Wu YF, Wang L, Li JY, Gao R, *et al*: PTPN2 inhibition disrupts mitochondrial renewal and blocks TFRC-Mediated mitophagy to exert Anti-Tumor activities in ALK-Positive anaplastic large cell lymphoma. Adv Sci (Weinh) 12: e14282, 2025.
25. Wang K, Shi X, Lin H, Xu T and Xu S: Selenium deficiency exacerbates ROS/ER stress mediated pyroptosis and ferroptosis induced by bisphenol A in chickens thymus. J Environ Sci (China) 148: 13-26, 2025.
26. Zhang X, Xu W, Wang Z, Liu J, Gong H and Zou W: Cross-talk between cuproptosis and ferroptosis to identify immune landscape in cervical cancer for mRNA vaccines development. Eur J Med Res 29: 602, 2024.
27. Liu J, Lichtenberg T, Hoadley KA, Poisson LM, Lazar AJ, Cherniack AD, Kovatich AJ, Benz CC, Levine DA, Lee AV, *et al*: An Integrated TCGA Pan-cancer clinical data resource to drive High-quality survival outcome analytics. Cell 173: 400-416.e11, 2018.
28. Wu T, Hu E, Xu S, Chen M, Guo P, Dai Z, Feng T, Zhou L, Tang W, Zhan L, *et al*: clusterProfiler 4.0: A universal enrichment tool for interpreting omics data. Innovation (Camb) 2: 100141, 2021.
29. Szklarczyk D, Gable AL, Lyon D, Junge A, Wyder S, Huerta-Cepas J, Simonovic M, Doncheva NT, Morris JH, Bork P, *et al*: STRING v11: Protein-protein association networks with increased coverage, supporting functional discovery in genome-wide experimental datasets. Nucleic Acids Res 47: D607-D613, 2019.
30. Otasek D, Morris JH, Bouças J, Pico AR and Demchak B: Cytoscape Automation: Empowering workflow-based network analysis. Genome Biol 20: 185, 2019.
31. Bader GD and Hogue CW: An automated method for finding molecular complexes in large protein interaction networks. BMC Bioinformatics 4: 2, 2003.
32. Lin H and Zelterman DJT: Modeling Survival Data: Extending the Cox Model. Technometrics 44: 85-86, 2002.
33. Livak KJ and Schmittgen TD: Analysis of relative gene expression data using real-time quantitative PCR and the 2(-Delta Delta C(T)) method. Methods 25: 402-408, 2001.
34. Wang L, Wang S and Li W: RSeQC: Quality control of RNA-seq experiments. Bioinformatics 28: 2184-2185, 2012.
35. Chen S, Zhou Y, Chen Y and Gu J: fastp: An ultra-fast all-in-one FASTQ preprocessor. Bioinformatics 34: i884-i890, 2018.
36. Kim D, Langmead B and Salzberg SL: HISAT: A fast spliced aligner with low memory requirements. Nat Methods 12: 357-360, 2015.
37. Anders S, Pyl PT and Huber W: HTSeq-a Python framework to work with high-throughput sequencing data. Bioinformatics 31: 166-169, 2015.
38. Love MI, Huber W and Anders S: Moderated estimation of fold change and dispersion for RNA-seq data with DESeq2. Genome Biol 15: 550, 2014.
39. Ginestet C: ggplot2: Elegant graphics for data analysis. J Royal Stat Soc Series A Statistics Soc 174: 245-246, 2011.

40. Wan Z, Wen M, Zheng C, Sun Y, Zhou Y, Tian Y, Xin S, Wang X, Ji X, Yang J, *et al*: Centromere protein F in tumor biology: Cancer's Achilles heel. Cancer Med 14: e70949, 2025.
41. Li RQ, Yang Y, Qiao L, Yang L, Shen DD and Zhao XJ: KIF2C: An important factor involved in signaling pathways, immune infiltration, and DNA damage repair in tumorigenesis. Biomed Pharmacother 171: 116173, 2024.
42. Burns M and Borgal L: Asp/ASPM phospho-regulation throughout the cell cycle. Genome 68: 1-10, 2025.
43. Marima R, Hull R, Penny C and Dlamini Z: Mitotic syndicates Aurora Kinase B (AURKB) and mitotic arrest deficient 2 like 2 (MAD2L2) in cohorts of DNA damage response (DDR) and tumorigenesis. Mutat Res Rev Mutat Res 787: 108376, 2021.
44. Tokuzumi A, Fukushima S, Miyashita A, Nakahara S, Kubo Y, Yamashita J, Harada M, Nakamura K, Kajihara I, Jinnin M and Ihn H: Cell division cycle-associated protein 1 as a new melanoma-associated antigen. J Dermatol 43: 1399-1405, 2016.
45. Malireddi RKS, Kesavardhana S and Kanneganti TD: ZBP1 and TAK1: Master regulators of NLRP3 Inflammasome/Pyroptosis, apoptosis, and necroptosis (PAN-optosis). Front Cell Infect Microbiol 9: 406, 2019.
46. Lin JF, Hu PS, Wang YY, Tan YT, Yu K, Liao K, Wu QN, Li T, Meng Q, Lin JZ, *et al*: Phosphorylated NFS1 weakens oxaliplatin-based chemosensitivity of colorectal cancer by preventing PANoptosis. Signal Transduct Target Ther 7: 54, 2022.
47. Lin C, Lin P, Yao H, Liu S, Lin X, He R, Teng Z, Zuo X, Li Y, Ye J and Zhu G: Modulation of YBX1-mediated PANoptosis inhibition by PPM1B and USP10 confers chemoresistance to oxaliplatin in gastric cancer. Cancer Lett 587: 216712, 2024.
48. Tan YT, LiT, Wang RB, Liu ZK, Ma MY, Huang RZ, Mo HY, Luo SY, Lin JF, Xu RH and Ju HQ: WTAP weakens oxaliplatin chemosensitivity of colorectal cancer by preventing PANoptosis. Cancer Lett 604: 217254, 2024.
49. Qi H, Li X, Ma J, Sun J, Liu Y, Wang X, Fan K, Shu C and Wang C: Fullerenols hijack lysosomes to disrupt inter-organellar crosstalk and block autophagy pre-activated by mTOR inhibitors for cancer cell PANoptosis. Sci Bull (Beijing) 70: 1275-1294, 2025.
50. Luo Y, Linghu M, Luo X, Li D, Wang J, Peng S and Ma Y: Remodeling tumor immunosuppressive microenvironment through dual activation of immunogenic panoptosis and ferroptosis by H2S-amplified nanoformulation to enhance cancer immunotherapy. Acta Pharm Sin B 15: 1242-1254, 2025.
51. Wang J, Chen Y, Xu Y, Zhang J, Yang S, Zhou Y, Lei J, Ren R, Chen Y, Zhao H, *et al*: DNASE1L3-mediated PANoptosis enhances the efficacy of combination therapy for advanced hepatocellular carcinoma. Theranostics 14: 6798-6817, 2024.
52. Wang S, Song A, Xie J, Wang YY, Wang WD, Zhang MJ, Wu ZZ, Yang QC, Li H, Zhang J and Sun ZJ: Fn-OMV potentiates ZBP1-mediated PANoptosis triggered by oncolytic HSV-1 to fuel antitumor immunity. Nat Commun 15: 3669, 2024.
53. Xing J, Ma X, Yu Y, Xiao Y, Chen L, Yuan W, Wang Y, Liu K, Guo Z, Tang H, *et al*: A Cardiac-targeting and anchoring bimetallic cluster nanozyme alleviates Chemotherapy-induced cardiac ferroptosis and PANoptosis. Adv Sci (Weinh) 12: e2405597, 2025.
54. Zhang J, Chen S, Wei S, Cheng S, Shi R, Zhao R, Zhang W, Zhang Q, Hua T, Feng D, *et al*: CircRAPGEF5 interacts with RBFOX2 to confer ferroptosis resistance by modulating alternative splicing of TFRC in endometrial cancer. Redox Biol 57: 102493, 2022.
55. Wei XB, Jiang WQ, Zeng JH, Huang LQ, Ding HG, Jing YW, Han YL, Li YC and Chen SL: Exosome-derived lncRNA NEAT1 exacerbates Sepsis-associated encephalopathy by promoting ferroptosis through Regulating miR-9-5p/TFRC and GOT1 axis. Mol Neurobiol 59: 1954-1969, 2022.
56. Feng G, Arima Y, Midorikawa K, Kobayashi H, Oikawa S, Zhao W, Zhang Z, Takeuchi K and Murata M: Knockdown of TFRC suppressed the progression of nasopharyngeal carcinoma by downregulating the PI3K/Akt/mTOR pathway. Cancer Cell Int 23: 185, 2023.
57. Mu Y, Sun J, Li Z, Zhang W, Liu Z, Li C, Peng C, Cui G, Shao H and Du Z: Activation of pyroptosis and ferroptosis is involved in the hepatotoxicity induced by polystyrene microplastics in mice. Chemosphere 291: 132944, 2022.
58. Zhang Y, Hu M, Jia W, Liu G, Zhang J, Wang B, Li J, Cui P, Li X, Lager S, *et al*: Hyperandrogenism and insulin resistance modulate gravid uterine and placental ferroptosis in PCOS-like rats. J Endocrinol 246: 247-263, 2020.
59. Urbańska K and Orzechowski A: Unappreciated role of LDHA and LDHB to control apoptosis and autophagy in tumor cells. Int J Mol Sci 20: 2085, 2019.
60. Shi X, Chen Y, Liu Q, Mei X, Liu J, Tang Y, Luo R, Sun D, Ma Y, Wu W, *et al*: LDLR dysfunction induces LDL accumulation and promotes pulmonary fibrosis. Clin Transl Med 12: e711, 2022.
61. Yao X and Li C: Lactate dehydrogenase A mediated histone lactylation induced the pyroptosis through targeting HMGB1. Metab Brain Dis 38: 1543-1553, 2023.
62. Lin S, Tan L, Luo D, Peng X, Zhu Y and Li H: Linc01278 inhibits the development of papillary thyroid carcinoma by regulating miR-376c-3p/DNM3 axis. Cancer Manag Res 11: 8557-8569, 2019.
63. Rong Y, Gao J, Kuang T, Chen J, Li JA, Huang Y, Xin H, Fang Y, Han X, Sun LQ, *et al*: DIAPH3 promotes pancreatic cancer progression by activating selenoprotein TrxR1-mediated antioxidant effects. J Cell Mol Med 25: 2163-2175, 2021.
64. Han F, Cheng C, Xu Q, Chen J, Yang Z and Liu J: DEPDC1B promotes colorectal cancer via facilitating cell proliferation and migration while inhibiting apoptosis. Cell Cycle 22: 131-143, 2023.
65. Li C, Liu Z, Kong D, Li Z and Li L: Lactylation: A novel driver of drug resistance in the tumor microenvironment. Cancer Drug Resist 8: 39, 2025.
66. Yang Y, Wu Y, Chen H, Xu Z, Lu R, Zhang S, Zhan R, Xi Q and Jin Y: Research progress on the interaction between glucose metabolic reprogramming and lactylation in tumors. Front Immunol 16: 1595162, 2025.
67. She H, Zheng J, Zhao G, Du Y, Tan L, Chen ZS, Wu Y, Li Y, Liu Y, Sun Y, *et al*: Arginase 1 drives mitochondrial cristae remodeling and PANoptosis in ischemia/hypoxia-induced vascular dysfunction. Signal Transduct Target Ther 10: 167, 2025.
68. Gong T, Wang QD, Loughran PA, Li YH, Scott MJ, Billiar TR, Liu YT and Fan J: Mechanism of lactic acidemia-promoted pulmonary endothelial cells death in sepsis: Role for CIRP-ZBP1-PANoptosis pathway. Mil Med Res 11: 71, 2024.
69. Xu L, Ye Y, Gu W, Xu X, Chen N, Zhang L, Cai W, Hu J, Wang T, Chao H, *et al*: Histone lactylation stimulated upregulation of PSMD14 alleviates neuron PANoptosis through deubiquitinating PKM2 to activate PINK1-mediated mitophagy after traumatic brain injury. Autophagy 21: 1473-1491, 2025.
70. Peng X, He Z, Yuan D, Liu Z and Rong P: Lactic acid: The culprit behind the immunosuppressive microenvironment in hepatocellular carcinoma. Biochim Biophys Acta Rev Cancer 1879: 189164, 2024.
71. Mi K, Chen Z, He J, Jiang C, Xia Y and Peng J: P300-Mediated ARRB1 lactylation promotes mitochondrial dysfunction and neuronal apoptosis in subarachnoid hemorrhage via upregulating S100A9. Neurochem Res 50: 174, 2025.
72. Du S, Zhang X, Jia Y, Peng P, Kong Q, Jiang S, Li Y, Li C, Ding Z and Liu L: Hepatocyte HSPA12A inhibits macrophage chemotaxis and activation to attenuate liver ischemia/reperfusion injury via suppressing glycolysis-mediated HMGB1 lactylation and secretion of hepatocytes. Theranostics 13: 3856-3871, 2023.